Exploring Dipole-Quadrupole Combined Function Magnets for a Muon Collider

Daniel Novelli, Luca Alfonso, Andrea Bersani, Luca Bottura, L. Brouwer, Barbara Caiffi, Stefania Farinon, Francesco Mariani, Samuele Mariotto, Alessandra Pampaloni, Tiina Salmi, and Y. Yan, *Member, IEEE*

***Abstract*—Over the past few years, interest in a Muon Collider as a potential post-LHC machine has grown significantly. By colliding muons, it is possible to achieve both precision and high energy, overcoming the limitations of synchrotron radiation in conventional lepton colliders. However, the very short muon lifetime at rest requires high beam intensity and fast acceleration rates limiting the collider ring dimensions. These limitations lead to several challenges in the design of superconducting magnets, which must generate high magnetic fields in large apertures to provide shielding from the radiation due to muon decay. This work explores the design of combined function magnets, which are essential to address the neutrino flux issue in straight sections by bending the particles during focusing/defocusing stages. The superconducting material selected for these magnets is REBCO, a High Temperature Superconductor (HTS), with operating temperatures ranging from 4.5 K to 20 K. Various configurations of combined function magnets are studied and simulated using a Python code interfaced with the Finite Element Method (FEM) software ANSYS, employing the sector coil approximation. The goal is to identify feasible designs that can accommodate substantial internal shielding while continuing to provide the high fields and gradients demanded by the lattice optics. To validate the manufacturability of such concepts, a preliminary winding test has been performed using Nb_3Sn in a Canted-Cosine-Theta (CCT) geometry. While REBCO represents the most promising HTS conductor for future high-field applications, Nb_3Sn remains one of the most mature options for large accelerator magnets, providing a valuable feasibility benchmark.**

***Index Terms*—Superconducting magnets, accelerator dipole, accelerator quadrupole, accelerator magnets, muon collider.**

I. Introduction

THE Muon Collider has recently emerged as one of the most promising options for a next-generation high-energy physics facility. By colliding muons instead of electrons or protons, it combines the energy reach of hadron colliders with the precision of lepton colliders, potentially extending the exploration frontier beyond the capabilities of the High-Luminosity LHC [1], [2]. With a mass of $m_\mu = 105.7\,\mathrm{MeV}/c^2$, about 200 times heavier than the electron mass ($m_e = 0.511\,\mathrm{MeV}/c^2$), muons experience synchrotron radiation losses reduced by a factor of 10^9 compared to electrons. The main challenge, however, lies in their extremely short lifetime at rest, only $2.2\,\mu$s, which imposes the need to produce, cool, accelerate, and collide them as quickly as possible [3]. The main decay channels of muons and antimuons are:

$$\mu^- \to \nu_\mu\, e^-\, \bar{\nu}_e \quad \text{and} \quad \mu^+ \to \bar{\nu}_\mu\, e^+\, \nu_e. \tag{1}$$

Electrons (e^-) and positrons (e^+) produced in muon decays must be absorbed locally by dedicated shielding to prevent quench and radiation damage to the superconducting magnet coils. In contrast, the emitted neutrinos (ν_μ, $\bar{\nu}_\mu$, ν_e, $\bar{\nu}_e$) interact only weakly with matter and therefore escape the collider tunnel, reaching the atmosphere. In the straight sections of the collider, the decay products of relativistic muons are emitted within a narrow cone with an angle $1/\gamma$, where γ is the Lorentz factor (see Fig. 1). As a consequence, neutrinos emerge from the tunnel in collimated beams carrying high energy, potentially leading to non-negligible equivalent radiation doses at ground level. One possible mitigation strategy consists in reducing the length of straight sections by introducing a controlled bending of the beam also during the focusing and defocusing phases. In this way, the neutrino emission is spread over a larger solid angle, lowering the radiation levels at the surface. This approach can be implemented by employing *combined-function magnets*, which simultaneously provide dipole and quadrupole fields within the same aperture [5].

This paper presents the progress made in the study of dipole–quadrupole combined-function magnets for the muon collider ring, focusing on their electromagnetic optimization, technological feasibility, and preliminary winding tests as practical validation studies.

Received 13 October 2025; revised 17 December 2025; accepted 6 January 2026. Date of publication 29 January 2026; date of current version 4 February 2026. *(Corresponding author: Daniel Novelli.)*

Daniel Novelli and Alessandra Pampaloni are with INFN-Genova, 16146 Genova, Italy, and also with the Sapienza University of Rome, 00185 Rome, Italy (e-mail: daniel.novelli@ge.infn.it; alessandra.pampaloni@ge.infn.it).

Luca Alfonso, Andrea Bersani, Barbara Caiffi, and Stefania Farinon are with INFN-Genova, 16146 Genova, Italy (e-mail: luca.alfonso@ge.infn.it; andrea.bersani@ge.infn.it; Barbara.Caiffi@ge.infn.it; stefania.farinon@ge.infn.it).

Luca Bottura is with the European Organization for Nuclear Research (CERN), 1211 Geneva, Switzerland (e-mail: luca.bottura@cern.ch).

L. Brouwer and Y. Yan are with Lawrence Berkeley National Laboratory (LBNL), Berkeley, CA 94720 USA (e-mail: lnbrouwer@lbl.gov; YufanYan@lbl.gov).

Francesco Mariani is with the Sapienza University of Rome, 00185 Rome, Italy, and also with INFN-LASA, 20090 Milan, Italy (e-mail: fr.mariani@uniroma1.it).

Samuele Mariotto is with the University of Milan, 20122 Milan, Italy, and also with INFN-LASA, 20090 Milan, Italy (e-mail: samuele.mariotto@mi.infn.it).

Tiina Salmi is with Tampere University, 33720 Tampere, Finland (e-mail: tiina.salmi@tuni.fi).

Color versions of one or more figures in this article are available at https://doi.org/10.1109/TASC.2026.3656869.

Digital Object Identifier 10.1109/TASC.2026.3656869

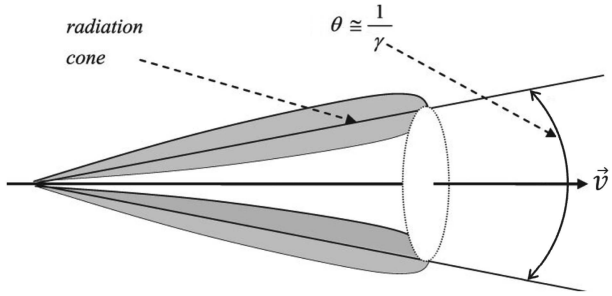

Fig. 1. The radiation cone produced by a charged particle moving at ultra-relativistic speeds while accelerating in the same direction as its motion [4].

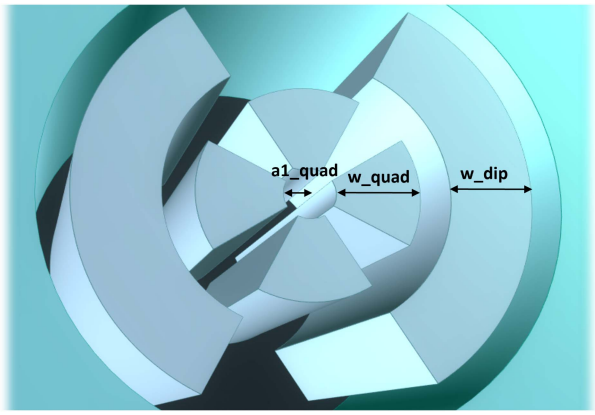

Fig. 2. Schematic representation of the geometrical variables: $a_{1,quad}$ (aperture radius), w_{quad} (quadrupole coil width), and w_{dip} (dipole coil width).

II. Python–Ansys Interface

The main goal of this work is to extend the performance-limit analysis of the collider ring magnets [6] to the case of combined-function configurations. Unlike standalone dipoles and quadrupoles, these magnets simultaneously generate two main field components of different orders within the same aperture, making it difficult to establish a general analytical formulation. For this reason, the study has been carried out by means of Finite Element Method (FEM) simulations using Ansys APDL. The aim is to reproduce the same workflow already developed for standalone dipoles [7] and quadrupoles [8], extending it to combined-function magnets in order to generate performance-limit maps that enable a direct comparison between multiple configurations in terms of field, gradient, and aperture.

A. Preliminary Analysis

To generate a magnetic field with two independent harmonic components, B_1 and B_2, a comparison among possible coil layouts was performed. Asymmetric coils, in which the secondary harmonic is introduced as a perturbation of the main one, are not suitable because they do not allow precise control of both field amplitudes. A more effective solution is the nested configuration, where one magnet is placed inside the other (Fig. 2). A comparative analysis between the two possible schemes — dipole inside quadrupole and quadrupole inside dipole — confirms that the configuration with the quadrupole placed inside the dipole provides higher overall efficiency, in agreement with US-MAP studies [9]. This is mainly because, for the same field at the winding, a quadrupole located at a smaller radius generates a higher gradient, whereas the magnitude of the dipole field is not sensitive to the coil radius. Consequently, the configuration with the dipole inside and the quadrupole outside results in a less efficient use of the available space. In addition, beam optics requirements for the Muon Collider typically demand stronger quadrupole gradients than dipole fields [10], as summarized in Table I.

TABLE I
Beam Physics Requirements for Combined-Function Dipole–Quadrupole Magnets in the Lattice Version 0.7 [10]

Dipole field	Quadrupole gradient	Aperture	Section
8 T	100 T/m	310 mm	Final Focusing
8 T	320 T/m	130 mm	Arc
4 T	240 T/m	170 mm	Matching
4 T	330 T/m	130 mm	Matching

B. Development of the Numerical Tool

A Python–Ansys interface was implemented to automatically run simulations and collect the main results after each iteration, allowing fast parametric exploration of different coil geometries and operating conditions without manual intervention. The study adopted a cos–theta configuration under the sector-coil approximation for both dipole and quadrupole windings [11]. The aim of the simulation campaign was to explore the trade-off between dipole field, quadrupole gradient, and aperture size, identifying feasible regions that satisfy the main technological constraints in terms of operational margin, mechanical stress, and quench protection. Within this framework, the main geometrical parameters were varied: the inner coil aperture radius $a_{1,quad}$, the quadrupole coil width w_{quad}, and the dipole coil width w_{dip}, as shown in Fig. 2. Therefore, a Python code with three different loops was developed to perform FEM simulations across the full parameter space. The aperture radius was varied from 25 mm to 150 mm in 25 mm steps, while for each aperture, the quadrupole coil width w_{quad} and dipole coil width w_{dip} were independently varied from 10 mm to 80 mm in 10 mm steps. For each geometry, electromagnetic and mechanical optimization cycles were performed to identify the configuration that maximizes the performance without crossing the critical surface or exceeding the maximum allowable azimuthal stress (400 MPa). As a baseline for the Muon Collider, HTS (REBCO) non-insulated (or metal-insulated) coils are considered, with three possible operating temperatures: 4.5 K, 10 K, and 20 K. This leads to 256 optimized configurations for each temperature. A cost model [12] is then applied to select only those solutions with an estimated cost below 400 kEUR/m per magnet, which is defined as the reference budget for the collider magnets.

Another key requirement for the collider magnets is a large aperture since they must host a tungsten absorber that limits the power reaching the coils at 4.5 K to 5 W/m, and up to

Fig. 3. 3D-printed radial build of the arc combined-function magnet. The main component in terms of size is the tungsten absorber (in silver).

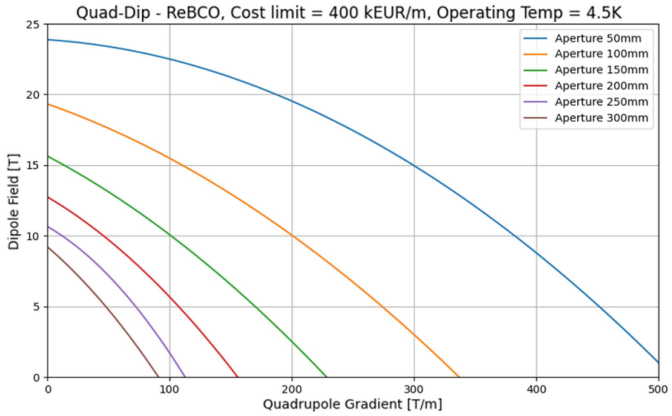

Fig. 4. B–G plot at 4.5 K for six different aperture diameters.

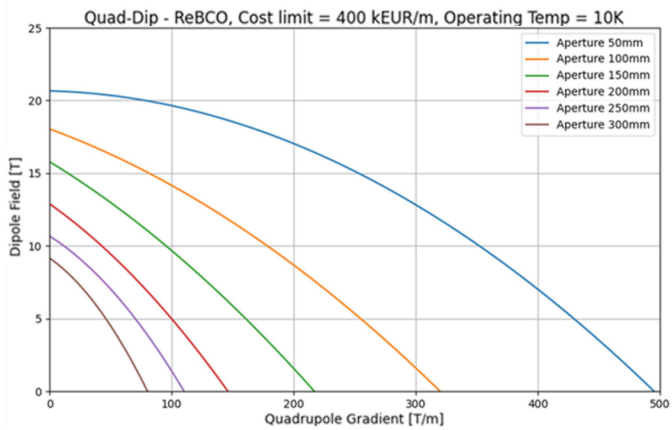

Fig. 5. B–G plot at 10 K for six different aperture diameters.

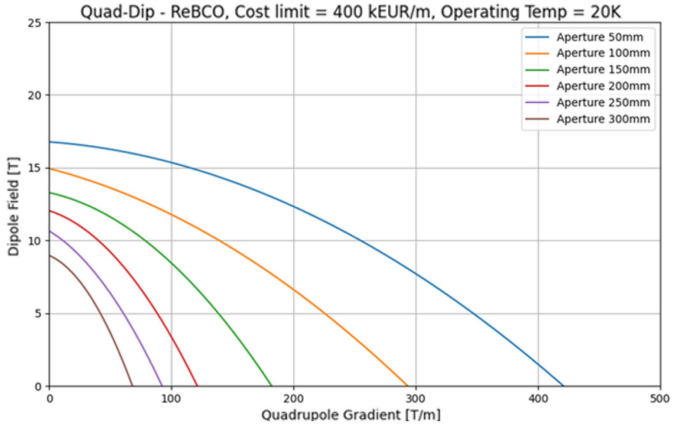

Fig. 6. B–G plot at 20 K for six different aperture diameters.

10 W/m for higher operating temperatures. This corresponds to a radial absorber thickness of about 4 cm and 3 cm, respectively, which represents the main reason why large coil apertures are necessary [13], [14]. Fig. 3 shows a 3D-printed sketch of the combined-function arc magnet, where the tungsten absorber clearly dominates the total coil aperture.

III. Performance Limits

By analyzing in detail the FEM simulations for all geometries, it was possible to identify a fitting curve for each aperture size in the so-called *B–G plots* — maps where the dipole magnetic field is plotted on the y-axis and the quadrupole gradient on the x-axis. Figs. 4, 5, and 6 show the B–G plots at 4.5 K, 10 K, and 20 K, respectively. In each plot, a limit curve can be identified as a function of the magnet aperture. This curve separates two regions: the area below the curve (allowed area), where the technological limits of superconducting magnets are satisfied, and the area above the curve (forbidden area), which corresponds to configurations that exceed one or more constraints related to mechanical stress, operating margin, or quench protection. As expected, increasing the operating temperature leads to a reduction in electromagnetic performance, but improves sustainability and reduces the overall environmental impact by avoiding the use of liquid helium. The intersections of the curves with the axes correspond to the configurations of a pure dipole (along the y-axis) and a pure quadrupole (along the x-axis).

These plots have proven to be a practical and effective tool to interface with beam-optics, establishing a common starting point for the design of the collider magnets. They make it possible to compare a large number of configurations in terms of aperture size and electromagnetic performance, and to identify the parameter space where feasible solutions may exist. However, a magnet lying in the allowed region is not necessarily guaranteed to be technically achievable, but it represents a realistic basis for further detailed design studies.

IV. Practical Studies

The baseline technology selected for the Muon Collider magnets is REBCO, considering that the project is foreseen to be realized in the coming years, allowing further R&D progress in HTS magnet technology. However, if such magnets were to be built with the technologies currently available, one of the most mature and effective options would be Nb_3Sn cables. Focusing on one representative combined-function magnet among those listed in Table I, namely the arc magnet (8 T, 320 T/m in a 130 mm

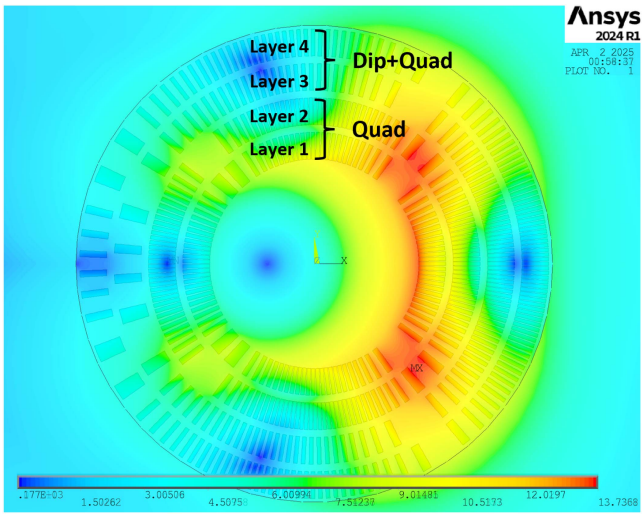

Fig. 7. 2D cross section of the arc dipole–quadrupole combined-function magnet, showing the magnetic field distribution and the adopted geometric layout.

aperture), the goal is to assess how far a Low-Temperature Superconductor (LTS) such as Nb_3Sn is from meeting the design target.

A. *Specific Design*

Among the possible magnet layouts, the Canted-Cosine-Theta (CCT) geometry was selected as the reference model. An electromagnetic design of a CCT magnet with a 130 mm aperture was therefore developed, consisting of four layers arranged in two layer pairs (see Fig. 7). In this study, the constraint of the nested configuration (quadrupole inside, dipole outside) was relaxed, allowing each layer pair to act independently as a dipole, quadrupole, or combined-function winding. Defining the ratio between the two desired harmonics as:

$$B_{\text{ratio}} = \frac{B_1\,[\text{T}]}{B_2\,[\text{T/m}] \cdot a_{1,\text{quad}}[m]} \tag{2}$$

the value of B_{ratio} is theoretically infinite for a pure dipole and zero for a pure quadrupole, while the design target corresponds to $B_{\text{ratio}} \approx 0.4$. Before proceeding with the winding tests, an optimization study was performed in Ansys to identify the configuration providing the best trade-off between dipole and quadrupole components within the given aperture. A design target of $B_{\text{ratio}} = 0.4$ led to a configuration consisting of a pure quadrupole in the first two layers ($B_{\text{ratio}} = 0$) and a combined-function winding in the two outer layers with $B_{\text{ratio}} = 1.4$, i.e., a dipole component stronger than the quadrupole one. The resulting layout was then selected as the reference for the electromagnetic model and reproduced in the laboratory. The conductor used is the Nb_3Sn Rutherford cable from the HL-LHC MQXF quadrupoles [15], with a bare width of 18.15 mm and a bare thickness of 1.53 mm. Operating at 4.2 K in the short-sample limit, the design achieves approximately half of the target performance, namely about 4 T and 160 T/m in the same aperture, with a peak field of 13.74 T located in the inner layers.

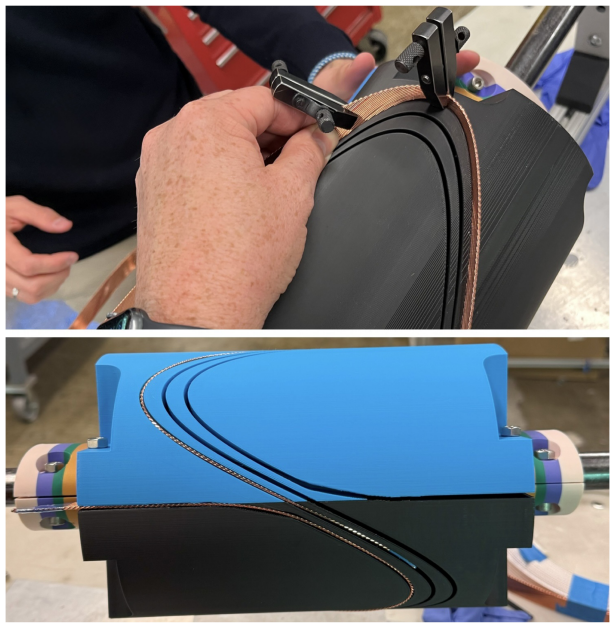

Fig. 8. Winding test on layer 1 of the CCT combined-function magnet.

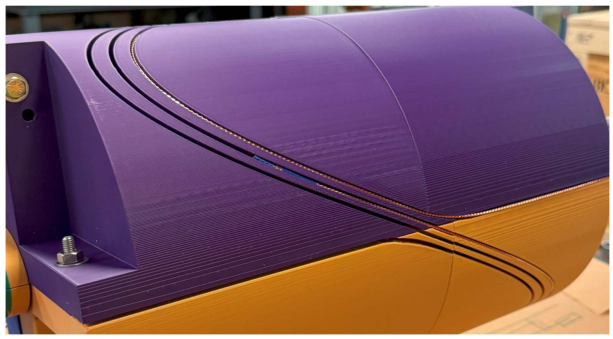

Fig. 9. Winding test on layer 3 of the CCT combined-function magnet.

B. *Winding Tests*

After the analytical and numerical study of the specific design, a CAD model was produced and 3D-printed mandrels were fabricated to perform winding tests. The goal was to visually inspect possible cable deformations; since no cryogenic testing was required, the mandrels were printed using PLA plastic. All groove parameters were optimized to minimize the critical aspects related to twist and bending angles in both easy- and hard-way directions, with a solenoid tilting angle of 25° selected to reduce the effects that can cause strand decabling in the Rutherford cable.

Fig. 8 shows the winding of layer 1, the most critical one due to its smaller radius. The fiberglass insulation was removed from the cable to allow visual inspection during the winding process. Small clamps were used to help prevent the strands from popping out of their grooves in the Rutherford cable. The winding test was successfully carried out, and the large aperture required by the Muon Collider design facilitated the operation. The process was stopped after the first turn in order to preserve the cable for further tests, as all turns are expected to behave identically.

An additional winding test was performed on layer 3, corresponding to the first combined-function layer, shown in Fig. 9. As expected, this operation was easier than the previous one, mainly due to the larger radius. The asymmetry introduced by the combined function coils did not create any particular difficulties, but it revealed the presence of a preferred cable orientation, which favors strand compaction rather than strand separation within the Rutherford.

V. Conclusion

The B–G plots provide the final step required by beam optics to define a new lattice that remains consistent with the technological limits of superconducting magnets. Although these plots were developed in the framework of the Muon Collider, the methodology itself is general. Beyond their analytical purpose, the B–G plots also represent a practical and effective tool for direct interaction with beam optics, providing an immediate way to identify realistic design targets. The allowed region should therefore be regarded as a starting point for detailed design studies [16], [17] rather than as an exclusive domain of feasible configurations.

In addition to the performance-limit study, practical investigations have been initiated on real Canted-Cosine-Theta (CCT) combined-function magnet configurations. The winding tests were successfully performed, demonstrating the windability and practical feasibility of this type of magnet design.

Acknowledgment

The authors would like to thank the PNRR_IRIS project of INFN funded by the Italian Ministry of Research for the financial support. The authors performed this work on behalf of IMCC.

References

[1] C. Accettura et al., "Towards a muon collider," *Eur. Phys. J. C*, vol. 83, 2023, Art. no. 864, doi: 10.1140/epjc/s10052-023-11889-x.

[2] D. Schulte, "The international muon collider collaboration," in *Proc. IPAC'21*, Campinas, Brazil, May 2021, pp. 3792–3795, doi: 10.18429/JACoW-IPAC2021-THPAB017.

[3] L. Bottura et al., "Magnets for a muon collider—needs and plans," *IEEE Trans. Appl. Supercond.*, vol. 34, no. 5, Aug. 2024, Art. no. 4005708, doi: 10.1109/TASC.2024.3382069.

[4] S. L. Prunty, "A primer on the theory of thomson scattering for high-temperature fusion plasmas," *Physica Scripta*, vol. 89, Nov. 2014, Art. no. 128001, doi: 10.1088/0031-8949/89/12/128001.

[5] K. Skoufaris, C. Carli, and D. Schulte, "10 TeV conter of mass energy muon collider," in *Proc. IPAC'22*, Bangkok, Thailand, Jun. 2022, pp. 515–518, doi: 10.18429/JACoW-IPAC2022-MOPOTK031.

[6] B. Caiffi et al., "Challenges and perspectives of the superconducting magnets for the muon collider storage ring," *IEEE Trans. Appl. Supercond.*, vol. 35, no. 5, Aug. 2025, Art. no. 4002007, doi: 10.1109/TASC.2025.3529424.

[7] D. Novelli et al., "Analytical evaluation of dipole performance limits for a muon collider," *IEEE Trans. Appl. Supercond.*, vol. 34, no. 5, Aug. 2024, Art. no. 4002405, doi: 10.1109/TASC.2024.3352526.

[8] D. Novelli et al., "Analytical and numerical study of superconducting dipole and Quadrupole performance limits for a muon collider," *IEEE Trans. Appl. Supercond.*, vol. 35, no. 5, Aug. 2025, Art. no. 4000205, doi: 10.1109/TASC.2024.3507744.

[9] V. V. Kashikhin, Y. Alexahin, N. V. Mokhov, and A. V. Zlobin, "High-field combined-function magnets for a 1.5 x 1.5 TeV muon collider storage ring," in *Proc. 12th Int. Part. Accel. Conf.*, 2012, pp. 3587–3589.

[10] M. Vanwelde, K. Skoufaris, and C. Carli, "Status of the 10 TeV center-of-mass collider lattice and IR design," in *Proc. IMCC Detect. MDI Workshop*, Jun. 2024.

[11] E. Todesco and P. Ferracin, "Limits to high field magnets for particle accelerators," *IEEE Trans. Appl. Supercond.*, vol. 22, no. 3, Jun. 2012, Art. no. 4003106, doi: 10.1109/TASC.2011.2181143.

[12] L. Bottura and B. Bordini, "HTS potential and needs for future accelerator magnets," 2025, *arXiv:2503.23048*.

[13] A. Lechner et al., "Radiation shielding studies for superconducting magnets in multi-TeV muon colliders," in *Proc. IPAC'24 Nashville, TN*, USA, May 2024, pp. 2536–2539, doi: 10.18429/JACoW-IPAC2024-WEPR26.

[14] D. Calzolari et al., "Radiation load studies for superconducting Dipole magnets in a 10 TeV muon collider," in *Proc. JACoW IPAC*, 2022, vol. 2022, pp. 1671–1674, doi: 10.18429/JACoW-IPAC2022-WEPOST001.

[15] P. Ferracin et al., "Magnet design of the 150mm aperture Low-β quadrupoles for the high luminosity LHC," *IEEE Trans. Appl. Supercond.*, vol. 24, no. 3, Jun. 2014, Art. no. 4002306, doi: 10.1109/TASC.2013.2284970.

[16] L. Alfonso et al., "Preliminary design of a block-coil magnet for the muon collider ring," *IEEE Trans. Appl. Supercond.*, vol. 35, no. 5, Aug. 2025, Art. no. 4000405, doi: 10.1109/TASC.2024.3510234.

[17] F. Mariani et al., "Preliminary electromagnetic and mechanical design of a cos($n\theta$) dipole for the muon collider study," *IEEE Trans. Appl. Supercond.*, vol. 35, no. 5, Aug. 2025, Art. no. 4000805, doi: 10.1109/TASC.2024.3519077.